Water Research 114 (2017) 122–134

Contents lists available at ScienceDirect

Water Research

journal homepage: www.elsevier.com/locate/watres

Development of a model to simulate groundwater inundation induced by sea-level rise and high tides in Honolulu, Hawaii

Shellie Habel [a, *], Charles H. Fletcher [a], Kolja Rotzoll [b], Aly I. El-Kadi [a, b]

[a] University of Hawai'i at Mānoa, School of Ocean and Earth Science and Technology, Department of Geology and Geophysics, POST Building, Suite 701, 1680 East-West Road, Honolulu, HI 96822, USA
[b] University of Hawai'i at Mānoa, Water Resources Research Center, 2540 Dole St., Holmes Hall 283, Honolulu, HI 96822, USA

ARTICLE INFO

Article history:
Received 6 December 2016
Received in revised form
15 February 2017
Accepted 16 February 2017
Available online 20 February 2017

Keywords:
Groundwater inundation
Sea-level rise
Groundwater modeling
Tidal flooding
Hazard assessment

ABSTRACT

Many of the world's largest cities face risk of sea-level rise (SLR) induced flooding owing to their limited elevations and proximities to the coastline. Within this century, global mean sea level is expected to reach magnitudes that will exceed the ground elevation of some built infrastructure. The concurrent rise of coastal groundwater will produce additional sources of inundation resulting from narrowing and loss of the vertical unsaturated subsurface space. This has implications for the dense network of buried and low-lying infrastructure that exists across urban coastal zones.

Here, we describe a modeling approach that simulates narrowing of the unsaturated space and groundwater inundation (GWI) generated by SLR-induced lifting of coastal groundwater. The methodology combines terrain modeling, groundwater monitoring, estimation of tidal influence, and numerical groundwater-flow modeling to simulate future flood scenarios considering user-specified tide stages and magnitudes of SLR.

We illustrate the value of the methodology by applying it to the heavily urbanized and low-lying Waikiki area of Honolulu, Hawaii. Results indicate that SLR of nearly 1 m generates GWI across 23% of the 13 km^2 study area, threatening $5 billion of taxable real estate and 48 km of roadway. Analysis of current conditions reveals that 86% of 259 active cesspool sites in the study area are likely inundated. This suggests that cesspool effluent is currently entering coastal groundwater, which not only leads to degradation of coastal environments, but also presents a future threat to public health as GWI would introduce effluent at the ground surface.

1. Introduction

Ongoing sea-level rise (SLR) poses a significant threat to evolving coastal municipalities and mega-cities initially developed under the misconception that sea-level would remain approximately stationary (Gornitz et al., 2001; Nicholls, 1995; Spanger-Siegfried et al., 2014). However, it is now understood that even marginal increases in sea-level are cause for concern as, in the United States alone, 3.7 million people live within 1 m elevation of their respective local high tide datum (Strauss et al., 2012). Over the 20th century, sea-level rose at a rate of 1.2 ± 0.2 mm/yr, and from 1993 to 2016 accelerated to a rate of 3.4 ± 0.4 mm/yr (Nerem et al., 2010). Initial ramifications are already being observed in the form of tidal flooding and decreased drainage. In parts of New York City, streets flood so regularly that residents joke about giving children wading boots for Christmas, and cars require regular brake and muffler changes due to frequent contact with saltwater (Gregory, 2013). In Norfolk, Virginia, vertical rulers have been installed along low-lying streets so that drivers can assess flood-water depth (Gillis, 2016). And in Miami, Florida, some businesses have noted a 15% drop in revenue due to traffic rerouting around flooded areas (Spanger-Siegfried et al., 2014; Prothero, 2013). Such flooding is expected to increase in frequency and magnitude; for instance, by 2040 it is projected that Washington D.C. will experience 388 tidal floods per year, not considering the contribution from rainfall, amounting to multiple flood events per day (Spanger-Siegfried et al., 2014).

Flooding concerns are further complicated by the interaction of coastal groundwater levels with sea level. Because coastal groundwater tables are generally above mean sea level and

* Corresponding author.
E-mail address: skey@hawaii.edu (S. Habel).

http://dx.doi.org/10.1016/j.watres.2017.02.035
0043-1354/

Abbreviations list

DEM	Digital Elevation Model
GWI	Groundwater Inundation
LiDAR	Light Detection and Ranging
LMSL	Local Mean Sea level
MMT	Monthly Maximum Tide Stage
NOAA	National Oceanic and Atmospheric Administration
OSDS	On-site sewage Disposal System
SLR	Sea level Rise

oscillations are closely tied to those of the ocean surface, groundwater tables rise by a similar magnitude as sea level rises, causing more flooding than predicted by hydrostatic modeling (Rotzoll and Fletcher, 2013). E.g., a scenario of 1-m SLR considering groundwater inundation (GWI) is expected to more than double the amount of flooding in Honolulu, Hawaii produced solely by marine inundation (Rotzoll and Fletcher, 2013). The threat of flooding is unique for each coastal municipality, hinging largely on the vertical extent of unsaturated space between built infrastructure and tidally-influenced coastal groundwater (Sweet and Park, 2014). As sea level rises, this space will narrow and in some places become lost altogether. This will produce GWI in the form of increasingly severe periodic localized flooding (Rotzoll and Fletcher, 2013) that will be exacerbated during periods of extreme high tide (Firing and Merrifield, 2004). Heavy rainfall is also likely to cause more extensive flooding owing to reduced unsaturated space available for infiltration and reduced run-off options (Horton, 1933).

As coastal groundwater levels rise with sea level and inevitably breach the elevation of built infrastructure, flood damage will ensue. Various components of underground infrastructure will be, and in some locations already are, the first utilities to be compromised by inundation (Sterling and Nelson, 2013; Veiga, 2014). The array of essential utilities affected includes sewer mains, storm drain systems, vented utility corridors, and on-site disposal systems (OSDS). Storm drain systems are subject to high water flooding that can impact urban activities. The potential for inundation of corroded sewer mains and OSDS is especially concerning owing to the likelihood of sewage-based contamination of groundwater. In regions such as the Hawaiian Islands where OSDS constitute a major component of sewage treatment, the coastal discharge of contaminated groundwater already presents a serious public health concern (Whittier and El-Kadi, 2014). As GWI becomes more widespread, contamination will expand across the ground surface, providing increased opportunity for public exposure (Balaraman, 2016).

Various offices in local and state government recognize that ongoing SLR will necessitate the development of adaptive design standards with regard to land-use policy, infrastructure, and hazard mitigation (NJDEP, 2013; NRC, 2011; Savonis et al., 2008; USACE, 2013). Adopting such standards is judicious; however, the lack of available hazard projections and site-specific mapping is a limiting factor and has been cited as one of the principal impediments to adaptation related policy (Bierbaum et al., 2013). The production of such hazard maps requires consideration of numerous distinct, yet interrelated regional characteristics that pertain to a municipality's SLR related flood risk. These include locally unique rates of SLR, tidal range, topography, water-table elevation, groundwater flow, and tidal-influence on groundwater.

The purpose of this study is to develop a methodology that can be used to simulate flood scenarios in urban municipalities resulting from inundation by tidally-influenced groundwater. The methodology goes beyond simple hydrostatic modeling that assumes flooding based solely on ground elevation relative to sea level. Here we account for the over-height of the groundwater table with respect to sea level and consider the decay of tidal efficiency with increasing distance from the coastline, which is generally overlooked in hydrostatic modeling. Further, we employ a quasi-three-dimensional groundwater model calibrated with a comprehensive collection of water level observations, which allows simulated water levels to vary in the cross-shore direction, an improvement compared to the one-dimensional simulation of water levels produced by Rotzoll and Fletcher (2013). The methodology mainly requires data that is publicly available for many regions including topographic and bathymetric LiDAR, water-level measurements, rates of groundwater withdrawals and recharge, and subsurface geology.

The model output can be seamlessly incorporated into geospatial platforms to compare with municipal geospatial data sets, toward identification of threatened infrastructure and quantification of future damage considering threatened taxable real estate. The output can also be displayed visually, providing decision-makers with a perspective of future scenarios. Specifically, the objectives of this methodology are to 1) gain an understanding of the hydrologic effects of SLR on coastal water-table elevations across a site-specific dense urban setting, 2) estimate the areal extent of GWI and expected narrowing of unsaturated space resulting from SLR-induced groundwater lift, and 3) produce maps that illustrate localized regions at risk of GWI resulting from SLR at a specified tide stage.

1.1. Study area: Waikiki, Oahu, Hawaii

For proof of concept, the method was applied to the Waikiki area on the island of Oahu, Hawaii. Waikiki is the gateway of Hawaiian tourism, accounting for nearly half of tourism statewide, supplying more than 72,000 jobs, and providing 8% of the gross state product (Department of Business (2003)). At present, the Waikiki coastal zone has generally narrow unsaturated space such that many construction projects working below the ground surface require dewatering of worksites. The conjunction of tidally-influenced groundwater and narrow unsaturated space produces localized temporary flooding during extreme tide events (Firing and Merrifield, 2004), requiring only a 20 cm tide above the mean higher high water datum to produce such flooding (Sweet, 2014). It follows that as SLR continues, unsaturated space will become progressively narrowed or eliminated altogether, resulting in chronic GWI.

1.1.1. Background

The study area is located on the southeastern side of the island of Oahu, Hawaii (Fig. 1). It is situated atop a low-lying coastal platform that is bounded to the northeast by an eroded and fragmented shield volcano known as the Koolau Volcano, to the east by a volcanic tuff cone known as Diamond Head Crater, to the west by Honolulu's principal seaport, Honolulu Harbor, and to the south by the coastline. A dredged, tidally influenced canal marks the landward border of Waikiki.

The southeastern coastal plain of Oahu is composed of a mixture of post-erosional volcanics, eroded alluvial debris from the Koolau Volcano and sedimentary deposits produced by Pleistocene sea-level variations including lagoonal deposits, coral debris, and coral ledges. These materials make up the geologic unit referred to as caprock, which lie atop the basalt of the Koolau Volcano (Finstick, 1996; Oki et al., 1998; Stearns and Vaksvik, 1935). Nearly the entire study area has been further overlain by heterogeneous human-

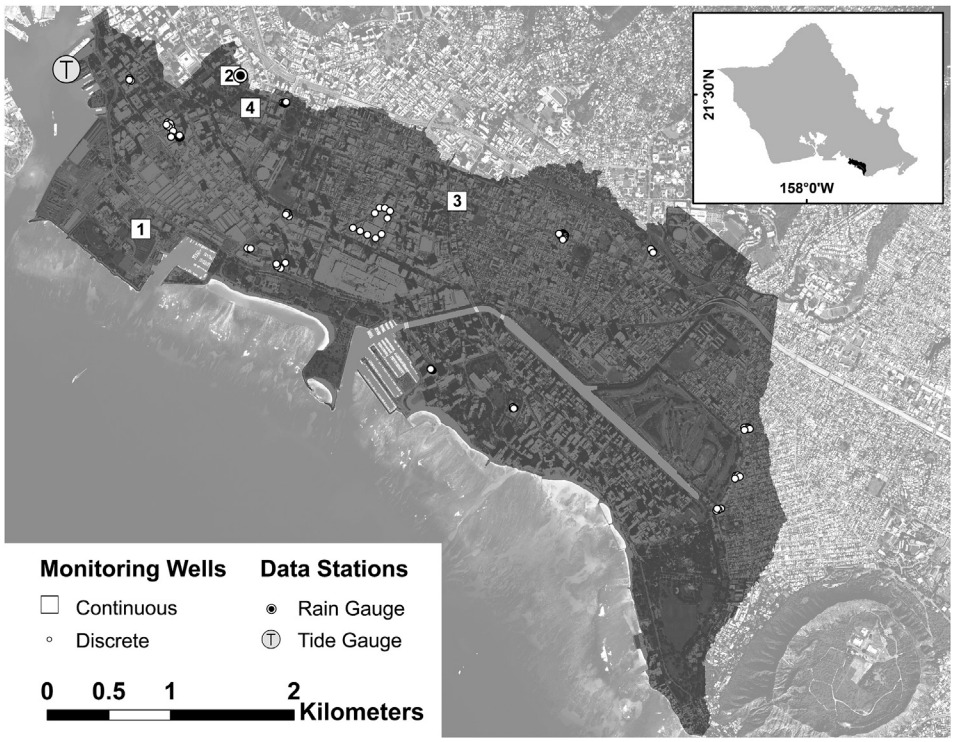

Fig. 1. Study area of Waikiki and surrounding commercial and residential districts on the island of Oahu, Hawaii. The shaded area shows the study region. Locations of wells from which water-level observations were obtained are shown.

placed fill consisting mainly of coralline sand and gravel (Finstick, 1996).

Groundwater within Oahu's southeastern coastal plain occurs primarily in the freshwater lens located in the basalt aquifer, and secondarily in caprock sediments (Gingerich and Oki, 2000). The freshwater lens floats atop saltwater due to density differences between salt and freshwater (Fig. 2) and with an interface that is roughly approximated by the Ghyben-Herzberg principle (Macdonald et al., 1983). Groundwater from the lens system migrates from inland recharge areas to coastal discharge areas (Souza and Voss, 1987). Lower permeability caprock acts as a semi-confining layer to the freshwater lens along the coastline by partially obstructing flow (Stearns, 1935).

Within the caprock aquifer, the uppermost limestone unit is unconfined and contains mainly brackish non-potable water that is highly vulnerable to contamination from the adjacent urban setting (Oki et al., 1998). Well withdrawal from the caprock aquifer is mainly employed for small-scale irrigation and for use in cooling towers (Whittier et al., 2010). Groundwater in the caprock aquifer is influenced by rainfall and marine oscillations generated by the tide and seasonal sea-level anomalies (Gonneea et al., 2013; Ponte, 1994; Wu et al., 1996; Yin et al., 2001). Marine oscillations become damped, decreasing in amplitude and increasing in lag as oscillations propagate further inland (Li and Barry, 2000).

Groundwater flow to the caprock aquifer occurs as water moves down-gradient from underlying basalt aquifers and discharges into

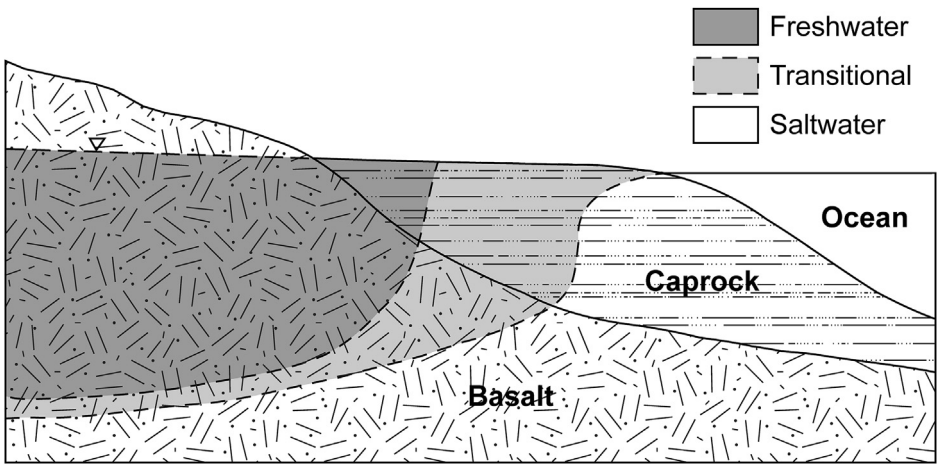

Fig. 2. Conceptual model of the freshwater lens located in the basalt aquifer and overlying caprock sediments of Oahu's southeastern coastal plain. The lens floats atop lower density saltwater and a transitional brackish boundary.

the caprock and the ocean. Surficial recharge to the caprock aquifer stems from infiltration of rainfall, water main leakage, septic leachate, seepage from reservoirs and cesspools, and irrigation (Engott et al., 2015).

1.1.2. Local sea-level rise

In Honolulu, the semi-diurnal tide range is 0.58 m and the local rate of SLR is 1.41 ± 0.21 mm/yr based on monthly mean sea-level measurements at the Honolulu tide station from 1905 to 2015 (NOAA a, 2016). Future acceleration in the rate of local sea level is expected to occur; however, the timing and magnitude of acceleration remain uncertain. Projections provided by the Fifth Assessment Report of the Intergovernmental Panel on Climate Change (IPCC) suggest that global mean sea level could reach 0.18–0.32 m by mid-century, 0.33–0.60 m by 2075, and 0.52–0.98 m by 2100 under Representative Concentration Pathway 8.5, the "business as usual" scenario (Church et al., 2013). However, simulations of globally relative rates of future SLR indicate that the component representing the redistribution of ice melt reaches the highest magnitude across the equatorial Pacific, resulting in rates of simulated local SLR in Honolulu exceeding 8 mm/yr over the second half of the century (Spada et al., 2013). Additionally, the contribution of ice melt solely from Antarctica has been reported as having the potential to contribute more than 1 m of sea-level rise by 2100 (DeConto and Pollard, 2016). These, and additional findings that global ice loss is exceeding researchers expectations, and that the tropical Pacific region is subject to SLR that will exceed global mean sea level rise, led Sweet et al. (2017) to develop regional SLR scenarios that significantly exceed IPCC projections. E.g., the Sweet et al. (2017) "Intermediate High" scenario for global mean sea level is 1.5 m by the end of the century, with an additional rise of approximately 0.5 m for the Hawaii region. Since global IPCC SLR projections likely underestimate future rates of local SLR in the Honolulu area, and are out of date with respect to sea-level studies that have been completed since the most recent IPCC report, the upper ranges of the IPCC projections are considered in the present case study and are referred to in terms of their magnitudes to preserve the relevance of simulation results as SLR projections evolve.

2. Methods

Our methodology toward assessing the effect of SLR on tidally-influenced water-table elevations and associated GWI includes six main components; 1) continuous groundwater-level monitoring, 2) compilation of groundwater-level measurements, 3) estimation of tidal efficiency, 4) development and calibration of a groundwater-flow model, 5) generation of flood maps, and 6) completion of a damage assessment. The following sections detail each component of the methodology.

2.1. Compilation of water-level measurements: continuous water level monitoring

Continuous observations of water level were taken to evaluate the influence of ocean oscillations on coastal water levels within the study area. Monitoring was accomplished at existing well sites established by the Department of Health Underground Storage Tank program. This federally mandated program manages privately and publicly owned underground storage tanks and installs shallow observation wells upon detection of contaminant leaks. The presence of these wells provides a unique opportunity to monitor water levels in heavily urbanized areas where monitoring opportunities would otherwise be limited.

The monitoring network employed in this study consisted of four shallow (<10 m depth) wells (Fig. 1), penetrating only the caprock, that were continuously monitored for several months at intervals ranging from 5 to 15 min. Data acquired during monitoring included groundwater pressure changes and temperature. The readings were converted from pressure measurements to water levels (m). The elevation of the ground surface at each well location was obtained using the nearest data point represented in 2013 NOAA LiDAR data (NOAA b, 2016). Elevations were not obtained through leveling due to the poor condition and control of benchmarks near well locations, thus providing reduced accuracy relative to the 2013 NOAA LiDAR dataset, which has 1 m horizontal resolution and 0.15 m vertical resolution. Ground elevations were used to reference groundwater levels relative to local mean sea level (LMSL).

Groundwater levels were compared to ocean levels to evaluate the influence of long-period (sea-level anomaly) and short-period (tidal) ocean oscillations at inland locations. Sea-level anomaly is the deviation of the non-tidal ocean level from LMSL that occurs over weeks and months. Ocean-oscillation data were recorded at 6-min intervals at the NOAA Honolulu, Hawaii tide station (Station 1612340) and referenced to LMSL (NOAA a, 2016) (Fig. 1). To separate tidal from sea-level anomaly oscillations, a weekly-moving average was applied to the tide-gage and groundwater data, which effectively removes the semi-diurnal and diurnal oscillations associated with the ocean tide. The weekly-moving average represents the sea-level anomaly, while the pure tidal signal is calculated by subtracting the sea-level anomaly from the tide-gage data. Groundwater levels were additionally compared to rainfall data for analysis of potential relationships to groundwater elevation. Rainfall data were acquired for the Beretania Pump Station (Network ID GHCND:USC00510211) (NOAA c, 2016), located within approximately 2 km of all monitoring sites.

The influence of ocean oscillations was quantified for each well by calculating tidal phase lag, and tidal and sea-level anomaly efficiency. The tidal phase lag was evaluated by cross correlating tidal signals at the Honolulu tide station with tidal signals observed in the groundwater data. Tidal efficiency, which describes the amplitude ratio between groundwater-level oscillations and ocean oscillations, was found using linear least-squares regression of lag-corrected groundwater time series to tidal-signal data. The slope of the regressed line quantifies tidal efficiency, while the y-intercept quantifies mean elevation of the groundwater level relative to mean ocean level.

Long-period oscillations of sea-level anomaly efficiency were found similarly using linear least-squares regression of weekly-moving averaged groundwater time series to sea-level anomaly data. The lag of the groundwater data to sea-level anomaly was too small to be considered. The tidal and sea-level anomaly efficiencies were used to remove both oscillations at the discrete measurements. For that purpose a linear least-squares regression of lag vs. distance of the observations from the coastline and exponential regressions of tidal and sea-level anomaly efficiencies vs. distance from the coastline were completed.

2.1.1. Compilation of water-level measurements: discrete observations

Ninety-five discrete water-level measurements (Fig. 1) that include information regarding time of measurement and surveyed elevation were acquired from Department of Health Leaky Underground Storage Tank records; measurements were taken between 1992 and 2008. Groundwater-level data were corrected with respect to the tidal efficiency, sea-level anomaly efficiency, and tidal lag as a function of distance from the coastline to represent the mean water level at that location. Groundwater levels corrected for ocean oscillations (wl_{corr}) at the lag corrected time of measurement

were calculated by:

$$wl_{corr} = wl - sl_{tide(T-Lx)}e^{ax} - sl_{anom}\, e^{bx},$$

where.

wl is the measured groundwater level (m relative to LMSL),
sl$_{tide}$ is the tidal signal (sea-level anomaly removed) at the time of the groundwater measurement corrected for tidal lag (m relative to LMSL),
sl$_{anom}$ is the sea-level anomaly (weekly moving average ocean oscillation) (m above LMSL),
a is the slope of the exponential relation between tidal efficiency and distance from the shoreline,
b is the slope of the exponential relation between sea-level anomaly efficiency and distance from the shoreline,
x is the distance from the shoreline (m).
T is the time the groundwater measurement was taken (local standard time: year, month, day, hour, min)
L is the slope of the linear relation between tidal lag and distance from the shoreline (min/m)

2.2. Groundwater model construction and calibration

A groundwater-flow model was developed to simulate steady-state water levels at LMSL in the unconfined caprock aquifer considering the current elevation of sea level and increases in sea level of 0.32 m, 0.60 m, and 0.98 m. Hydrologic characteristics used to construct the model were based on regional hydrologic studies (Oki, 2005), ranges in hydraulic conductivity observed within and near the study area (Finstick, 1996), and subsurface geology in the study area (Ferrall, 1976). The numerical model utilized MODFLOW-2005 (Harbaugh, 2005), a quasi-three dimensional cell-centered, finite difference, saturated-flow model.

2.2.1. Model grid withdrawals, and recharge

The model consisted of 443,602 active 10-m uniform grid cells and two layers, representing caprock and basalt hydrogeologic units. The top of the caprock unit was characterized using 2013 NOAA LiDAR topography data and 2013 U.S. Army Corps of Engineers LiDAR bathymetry data (NOAA b, 2016), while the bottom of the unit was characterized using contour data that defines the top elevation of the basalt aquifer (Rotzoll and El-Kadi, 2007). Details of the flow in the basalt aquifer unit are beyond the scope of this study. Therefore, such an aquifer was represented by a thin unit that extended an arbitrary 1 m below the base of the caprock and was included exclusively to simulate flow from the basalt into the caprock aquifer. Horizontal hydraulic conductivity for the second unit was defined as 600 m/d based on values reported in modeling studies that simulate local basalt aquifers (Rotzoll and El-Kadi, 2007; Izuka et al., 2016).

Well locations and withdrawal rates available from the State Commission on Water Resource Management were adopted from existing groundwater-flow models representative of the Honolulu aquifer (Rotzoll and El-Kadi, 2007). Only wells pumping from the caprock were considered. Well withdrawal rates were defined as the arithmetic mean of respective pumping rates from 1996 to 2005. Since pumping rates did not fluctuate significantly between 1996 and 2005, the average was considered an acceptable representation of the simulated period.

Recharge data were acquired from the mean annual water-budget model for the Island of Oahu, Hawaii (Engott et al., 2015), which is representative of average climate conditions, 1978 to 2007 rainfall, and 2010 land cover. The hydrological processes simulated in the water-budget model are rainfall, fog interception, irrigation, direct runoff, septic system leachate, and evapotranspiration.

2.2.2. Boundary conditions and simulation of SLR

The landward, seaward, and bottom boundaries were defined as no-flow boundaries and the upper boundary was defined as a recharge boundary. Flow from the bottom unit to the upper unit was simulated using a zonally-characterized general-head boundary for the bottom unit. Values of head defined for each zone were based on simulations of confined head in southern Oahu (Rotzoll and El-Kadi, 2007).

An additional general-head boundary was applied to the upper unit, extending seaward of the 0-m elevation contour, to represent sea-level elevation and coastline position. Increases in sea-level were simulated by raising the general-head boundary from 0 m to 0.32 m, 0.60 m, and 0.98 m for the chosen SLR scenarios, and by migrating the coastline position to corresponding contour lines.

2.2.3. Model calibration

Calibration accuracy was evaluated by comparing simulated against observed water levels. Several values of horizontal hydraulic conductivity applied to the caprock unit were estimated using the non-linear inverse modeling utility, PEST (Doherty, 2008).

As part of this approach, seven zones were characterized (Fig. 3) based on locations of distinct geologic units encountered within the subsurface (Ferrall, 1976). The hydraulic conductivity was defined for two zones prior to executing PEST; the zone labeled HK 50 was assigned a hydraulic conductivity of 1 m/d based on the abundance of cemented and fine grained sediments found offshore (Sherman et al., 1999, 2014). The zone labeled HK 30 was assigned a hydraulic conductivity of 65 m/d to replicate results of a drawdown test that had been conducted within the respective modeled zone (HBWS, 2005). All post-calibration values applied to the model were within the range of values observed inside or just to the west of the study area (Finstick, 1996).

Manual iterative adjustment was employed in the estimation of the conductance parameter of the general-head boundary defined for unit 2, and given a final value of 0.003 m^2/d. The general-head boundary conductance of unit 1 was pre-defined as 10 m^2/d. Following calibration, the mean residual water level and root-mean-squared error were 0.09 m and 0.12 m, respectively (Fig. 4).

2.2.4. Model assumptions and limitations

In general, numerical models have limitations owing to assumptions inherent in their conceptual design including the governing equations. Simplifications generally lead to overlooking or simplifying certain processes and to ignoring spatial and temporal variability of aquifer parameters. The specific limitations adopted in this study are summarized below.

Simulated steady-state conditions were modeled under the assumption that recharge, pumping, and groundwater flow remain constant. Simulations do not consider small-scale withdrawals that are currently employed across the study area for purposes including construction-site dewatering and mitigation of basement flooding. The simulation is not capable of assessing numerous time-dependent factors including short-term variations in recharge, pumping rates, and boundary flows. The model simulations represent conditions of 30-year average annual recharge and the tide stage relative to mean sea level. They do not include any consideration of anomalous conditions of extreme wet or dry periods or seasonal sea-level anomalies. However, the model results provide reasonable representation over a longer time frame considering the relatively slow subsurface water movement.

The MODFLOW-2005 model assumes a uniform density of water, which inhibits the model's capability to simulate the saltwater/freshwater interface, and hence, does not incorporate the influence

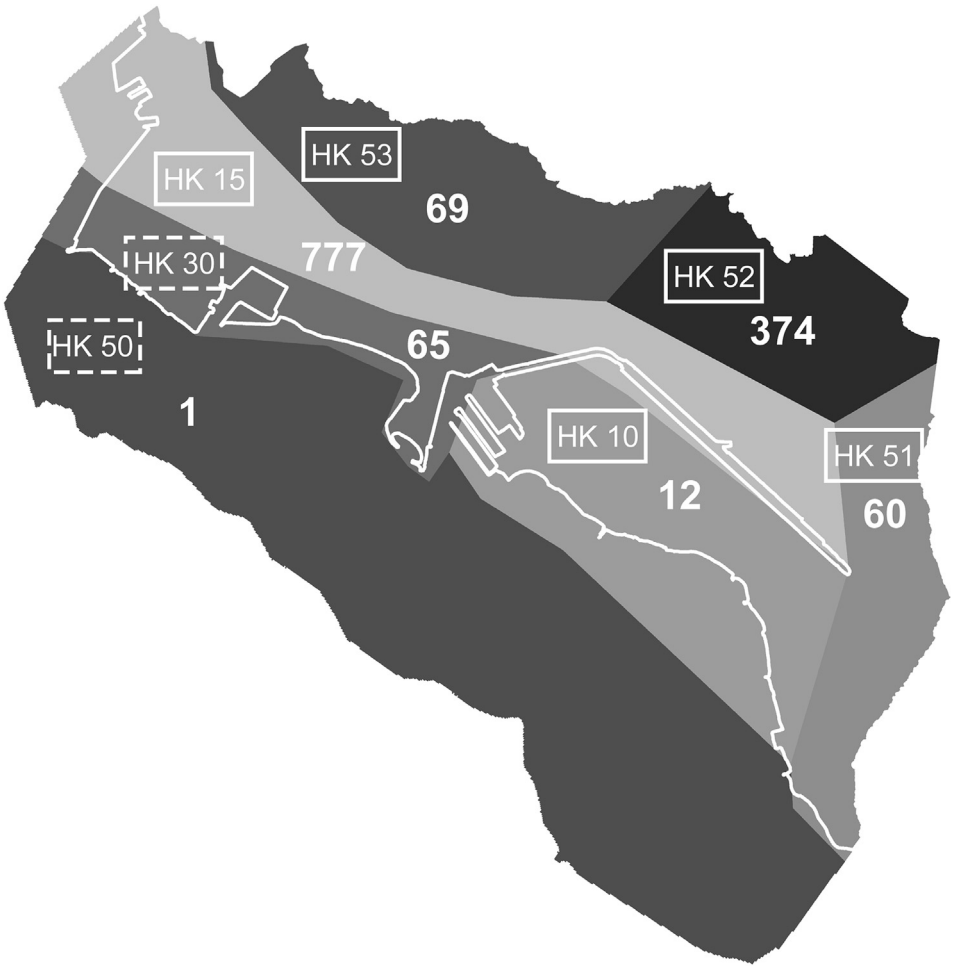

Fig. 3. Spatial distribution of parameter zones that characterize variations in hydraulic conductivity across the study area. Values of post-calibration hydraulic conductivity are reported in units of m/d; associated zone ID's are shown in white boxes where hydraulic conductivity was calculated using the zonal PEST approach, and in dashed boxes where hydraulic conductivity was defined by other means. The coastline and outer boundary are outlined for reference.

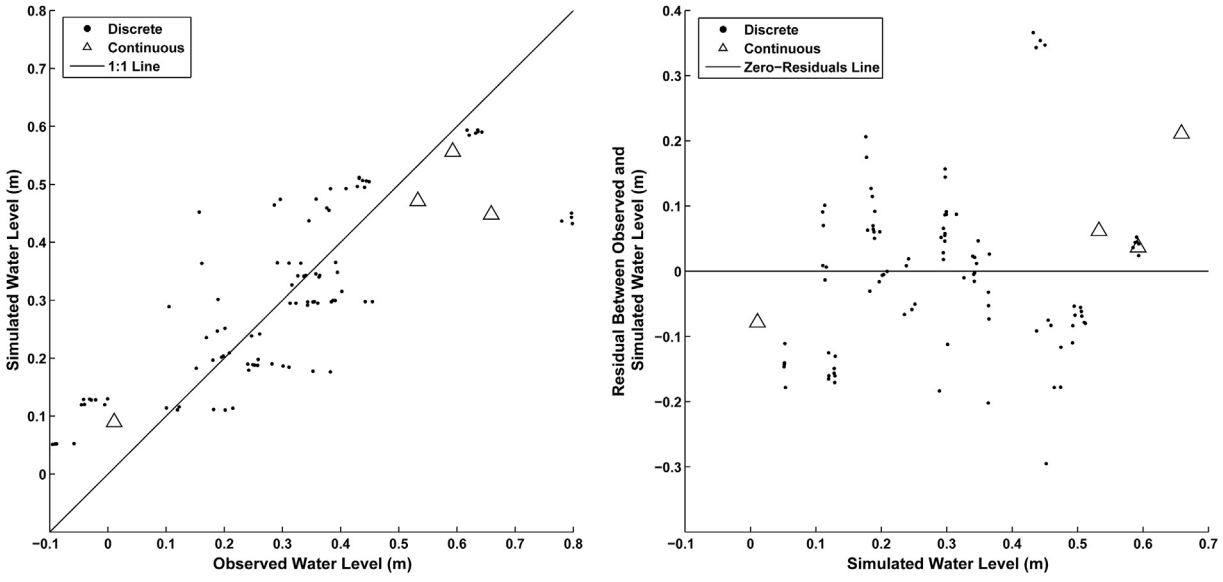

Fig. 4. Calibration plot showing observed vs. computed water levels and corresponding plot of residual vs. computed water levels. Discrete water levels are shown as circles and averages of continuous water levels are shown as triangles. Reference lines are included to represent the 1:1 correlation line and the zero-residuals line. The correlation coefficients for continuous and discrete water levels are 0.95 and 0.81, respectively.

of density driven fluid flow. Because the caprock aquifer is mainly brackish, the uniform density model was deemed reasonable for use in this study; however, the caprock aquifer does have a freshwater component, thus it would be worthwhile to collect salinity observations across the study area and employ SEAWAT (Langevin et al., 2003) or a similar variable-density groundwater flow model to improve future simulations.

Heterogeneity in groundwater environments is prevalent, especially in the caprock aquifer; however, heterogeneities across the study area are poorly understood and thus difficult to include in the design of the conceptual model. Hydrogeologic zones and units were simulated as homogeneous to avoid over-complicating the model, and because detailed hydrologic and geologic information is limited. Thus, heterogeneities in the caprock aquifer were not adequately represented.

Simulations of future conditions assume that GWI occurs when the water-table breaches the ground surface; the model does not account for subsequent surface flow, evaporation, or ponding that occurs due to breaching. The model also does not consider flow in the unsaturated zone, which can be relevant for fine materials. Also, what is termed here as unsaturated space is completely dry in the model simulation. With such an assumption, potential risk to utilities is actually underestimated since such areas are not completely dry.

2.3. GWI map generation

Digital data surfaces that characterize regions affected by GWI, and regions with severely narrow unsaturated space (defined here as having vertical thickness of less than 0.33 m), can be produced by quantifying vertical proximities between the local terrain and simulated water-table elevations. Local terrain can be simulated by constructing a digital-elevation model (DEM) from regionally specific topographic LiDAR data. Such data is available for many heavily urbanized regions, and can be acquired from NOAA (NOAA b, 2016).

For this study, a DEM was produced by merging and hydro-flattening 2013 NOAA DEM tiles. Raw ground return data points describing elevations relative to LMSL were used by NOAA to generate rasterized DEM tiles with 1-m horizontal resolution. The data has a linear error of 0.15 m; thus, the DEM has a similar linear error across regions defined by high-point density, and slightly higher error across regions defined by low-point density. Hydro-flattening was accomplished to ensure that water-reflected returns were excluded from the DEM by applying an arbitrary constant elevation of −1.5 m to all major waterways, water features, and offshore areas.

Rasterized representations of simulated water-tables were constructed by interpolating digital data structures from the xyz point data output of respective MODFLOW simulations. Digital data structures were produced using the triangulated irregular network method of interpolation and subsequently converted into 1×1 m raster grids.

Tidal influence was simulated by applying the 1-D analytical solution for tidal efficiency across a raster grid as a function of the distance of each raster cell from the modeled coastline. The raster grid was produced by calculating the distance of each cell from the 0-m elevation contour and applying the tidal efficiency component of the ocean-oscillation correction equation across the grid to arrive at tidal efficiency values from 0 to 1. The values of each cell were then multiplied by a given tide stage to simulate the tidal surplus. This raster data set was then summed with respective water-table raster data sets to arrive at the tidally-influenced water-table height at the given tide stage. The method can be used to simulate any stage within the local tidal range. For this study, the average monthly maximum tidal amplitude (MMT) measured at the Honolulu Tide Station (0.49 m) was chosen for simulation to represent a monthly flood event. The MMT is defined as average maximum monthly tide height measured over the 19-year National Tidal Datum Epoch. The current National Tidal Datum Epoch for the United States is 1983–2001.

The final step towards producing GWI maps quantifies the vertical extent of respective SLR-influenced water-table simulations relative to the local terrain. This was accomplished by subtracting each water-table raster grid from the DEM on a cell-by-cell basis. This process produced a series of raster grids in which positive cell values represent locations where the simulated water-table is situated below the modeled terrain and negative cell values where the simulated water-table is situated above the modeled terrain at extents specified by the cell value in meter units.

2.4. Uncertainty

Two main sources of error were identified in the uncertainty analysis for vertical disparity between the ground surface and potentiometric surface; these are LiDAR error and calibration MODFLOW error. Vertical error present in the LiDAR data was reported as less than 15 cm (Photo Science Inc., 2013). Error in the MODFLOW simulation was found to be 12 cm based on the root-mean-squared difference between simulated and observed water levels. Water levels and elevations were measured with sub-centimeter accuracy, thus measurement error is assumed to be insignificant compared with the MODFLOW simulation error. The quadrature sum of the two sources of vertical error (LIDAR and MODFLOW simulation) was found to be 20 cm. This measure of vertical uncertainty was used to quantify the lateral uncertainty in GWI rasters, which was accomplished by re-projecting flood and narrow unsaturated space contours (0.33 m relative to the groundwater level) above and below the respective simulated contours considering the 20 cm error. Additional uncertainties are present in the GEOID 12a model, which is used to transform heights between ellipsoidal coordinates and physical height systems. Within the study area, the vertical error in GEOID 12a ranges from 59 to 73.5 cm (Carlson, Personal communication). The analytical solution that was used to simulate elevated tide stages and to correct discrete groundwater levels considering influence by ocean-oscillations assumes uniform tidal and sea-level anomaly attenuation properties across a 1-D transect. Thus, the analytical solution does not account for cross-shore variation of the attenuation properties. Additional conditions that alter the vertical extent of the water-table, such as drought, prolonged precipitation and seasonal sea-level anomalies, were not included as part of the vertical uncertainty estimate as simulations are representative of average conditions of annual recharge at the MMT tide stage.

2.5. Damage assessment

To explore the utility of the GWI maps, a damage assessment was carried out that quantifies the extent of municipal infrastructure and taxable real estate threatened by projected increases in water-table elevation.

2.5.1. Taxable real estate

The value of threatened taxable real estate, considering structural assets and property, was assessed for each SLR scenario using the following data sets: 2015 tax data from the City and County of Honolulu's Real Property Assessment Division (CCH, 2016), geospatial data representing tax parcel locations (SHOP, 2016), and geospatial data characterizing building footprint locations (CCH, 2016). Tax data were merged with geospatial data based on individual parcels to link asset values to their corresponding locations.

Merged geospatial data were then compared to GWI raster grids to identify proportions of building areas and property areas affected by GWI. The total value of threatened property was assessed by multiplying each property value by the corresponding percent area affected by GWI and summing all products. The total value of threatened structural assets was quantified similarly; however, structure values representing only the first floor were considered by dividing each structure value by the corresponding number of floors. The sum of the overall threatened property value and overall threatened structure value was calculated to arrive at the total value of threatened taxable real estate.

2.5.2. Municipal infrastructure

The potential for roadway inundation was determined for each SLR scenario using a geospatial dataset that characterizes locations of Honolulu City and County Roadway acquired from the State of Hawaii Office of Planning (SHOP, 2016). The dataset was compared to GWI raster grids to quantify the total length of GWI affected roadway produced by each scenario.

The potential for OSDS inundation was evaluated for each SLR scenario using a geospatial dataset that characterizes active OSDS sites on the island of Oahu, acquired from the State of Hawaii Department of Health (Whittier and El-Kadi, 2009). The OSDS dataset was compared to GWI raster grids to quantify the number of both fully submerged sites and partially submerged sites lacking the 4.4 m unsaturated space required for cesspool construction according to Administrative Rule, Chapter 11–62 entitled "Wastewater Systems" (Department of Health (2004)). Here we consider fully submerged OSDS sites as potential sources of surface contamination, and partially inundated sites as potential sources of groundwater contamination based on the lack of unsaturated space necessary for sewage filtration. Many existing OSDS sites were constructed prior to the establishment of these requirements, thus their existence is legally allowed. However, it is prudent to identify potentially inundated sites based on the environmental ramifications that could result from direct seepage of raw sewage into groundwater and floodwater.

3. Results

3.1. Monitoring results

The influence of ocean oscillations and rainfall on water-table elevations at the four monitored well sites was investigated (Fig. 5). The corresponding tidal influence parameters were calculated for the four monitored sites (Table 1). The ocean-oscillation correction equation was derived excluding the anomalous value calculated for Well 3, yielding values of −0.0017 for $\boldsymbol{a}$, −0.0002 for $\boldsymbol{b}$, and 0.1215 for $\boldsymbol{L}$ with correlation coefficients of 0.96, 0.41, and 0.95, respectively.

The influence of tidal oscillations is evident at three of the monitored well sites, with generally higher influence at the site located nearer to the coastline. Water levels observed at Well 3 indicate heavy damping of the tidal signal and sharp increases during rainfall events, specifically during the large rainfall event in September of 2014. The location of Well 3 within a relict river channel suggests that the subsurface is likely comprised of fine grained or weathered material, which would explain the elevated water levels during rainfall events owing to reduced rates of infiltration and the damped tidal influence.

The influence of sea-level anomalies is evident at all four of the monitored well sites. Observations from Wells 1 and 4 feature particularly exceptional levels of correlation between long period variations in ocean and groundwater levels; this is based on sea-level anomaly efficiency values and plots of weekly-moving average ocean and water-table elevations that approximately mimic each other.

The continued rise in sea-level represents an extremely long period ocean oscillation relative to those observed as part of this study; thus, it is expected that corresponding sea-level anomaly efficiencies considering time periods of decades or centuries will be further elevated and will approach 1.0 across the study area. This level of efficiency would produce a nearly 1:1 relationship between magnitudes of SLR and long-term lifting of the coastal water-table.

3.2. Hydrologic modeling results

The simulation of current water-table elevations (Fig. 6) illustrates that groundwater levels generally increase with distance from the coastline. Due to the spatial aquifer variability, the relationship between water-table elevation and shoreline distance is spatially variable. The simulation also illustrates the influence of drawdown at locations where pumping is included in the model. Simulated water levels in the western coastal region of the study area appear to overestimate measured groundwater levels by as much as 18 cm, however these observations consist of anomalously low or negative water-table elevations and may indicate the presence of localized pumping or karst in the area. Simulated water levels adjacent to the eastern end of the canal appear to underestimate observed water levels by as much as 37 cm, likely owing to dynamic conditions of hydraulic gradient that may exist in this area. Simulations showing the influence of SLR on water-table elevations reinforce the assumption that increases in water-table elevations will be approximately equal to magnitudes of SLR.

3.3. Results of GWI mapping

Raster visualizations illustrate current and future conditions of GWI and narrow unsaturated space (Fig. 7). The simulation representing current conditions successfully reproduces water bodies that are present in the study area. However, small pockets of GWI are also simulated in areas not known to flood during the representative tide stage. The simulation was qualitatively compared with images taken of archeological survey trenches that confirm the presence of narrow unsaturated space in multiple regions in which they were simulated. Because discrete water levels and photographic evidence indicate that simulated water levels are consistent with observations, it is possible that the current extent of GWI is being alleviated through undocumented small scale pumping operations employed to dewater basements and construction sites.

Spatial calculations indicate that 1.1% of the 13 km^2 study area currently hosts unsaturated space narrower than 0.33 m. This extent increases to 5.7% in the +0.32 m scenario, 15.4% in the +0.60 m scenario, and 19.3% in the +0.98 m scenario (Fig. 8). The +0.98 m scenario also shows GWI across 23.0% of the study area, which resides mainly in places occupied by heavily used roadways.

3.4. Vulnerability assessment

Results of the vulnerability assessment (Table 2) suggest that more than $185 million of taxable real estate is currently exposed to flood waters during the MMT stage of the tide. This value increases exponentially over the three respective scenarios, reaching nearly $5 billion in the +0.98 m scenario. The length of inundated roadway also increases exponentially, covering 0.023 km in the current scenario and increasing to nearly 48 km in the +0.98 m scenario. Results of the OSDS site assessment suggest that 86% of the 259 total active sites present in the study area are not compliant

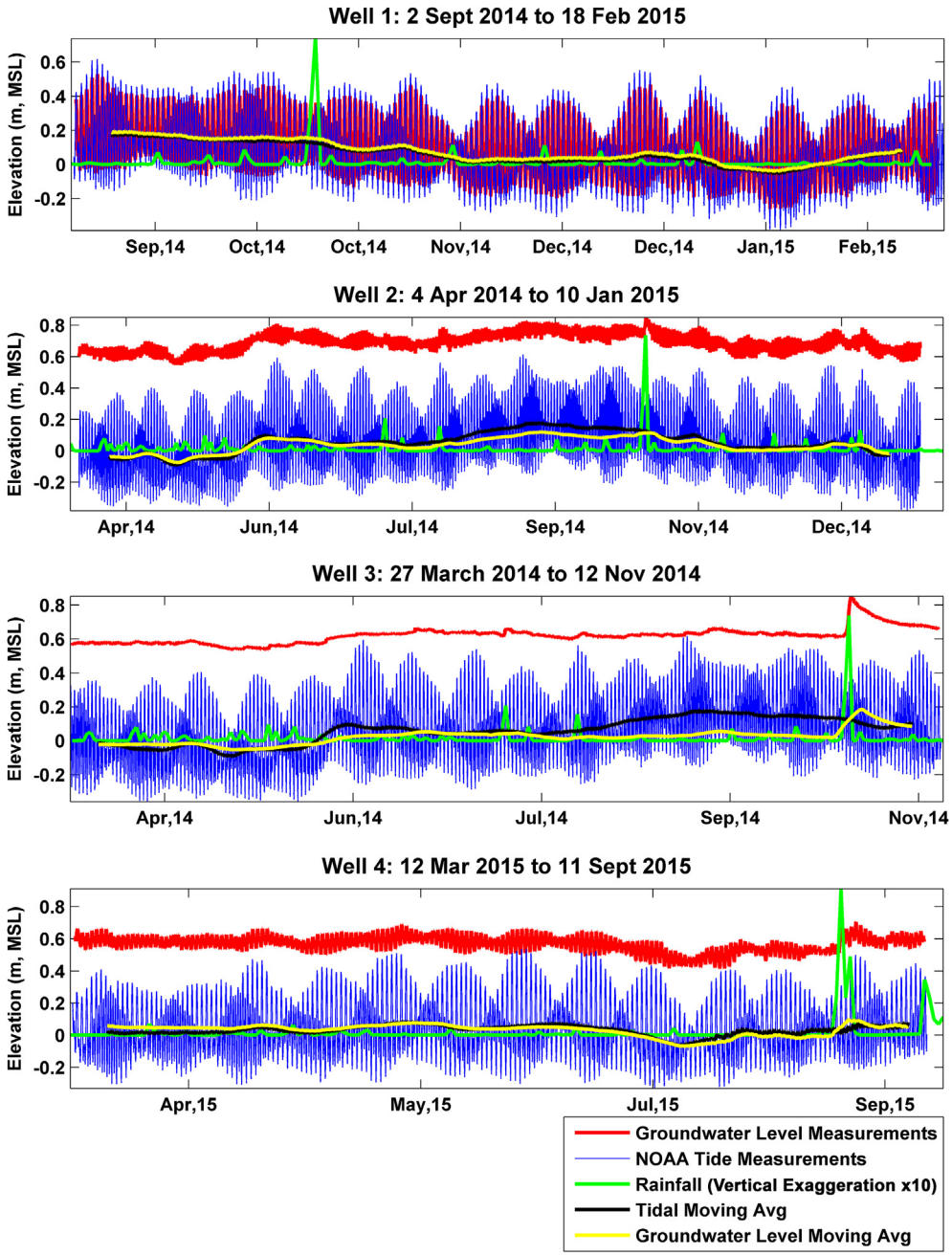

Fig. 5. Groundwater level observations at the four monitored well sites in order of shoreline proximity. Observations of rainfall in units of meters (×10 vertical exaggeration), the water level at the tide gage, and weekly-moving average values of ocean-level and groundwater-level observations (vertically displaced by respective values of offset for clarity).

Table 1
For each monitored well site, values of site distance from the coastline, vertical offset from LMSL, tidal lag, and tidal and sea-level anomaly efficiency are shown. Tidal lag and offset are correlated to coastal distance, while tidal efficiency is inversely correlated to coastal distance. Heterogeneities in the sediment cause deviation from these trends, and the variation in sea-level anomaly efficiency values.

	Distance to coast (m)	Tidal lag (min)	Tidal efficiency (m/m)	Sea-level anomaly efficiency (m/m)	Offset (m)
Well 1	232	45	0.75	1.02	0.01
Well 2	1042	135	0.13	0.69	0.66
Well 3	867	145	0.002	0.36	0.59
Well 4	1160	130	0.16	1.01	0.53

with current construction requirements, with one site shown as being fully submerged. Results considering the +0.98 m scenario indicate that the percentage of non-compliant OSDS sites increases to more than 91%, with 39 sites fully submerged.

4. Discussion

This study illustrates the utility of a methodology to identify localized GWI and municipal vulnerabilities that will result from

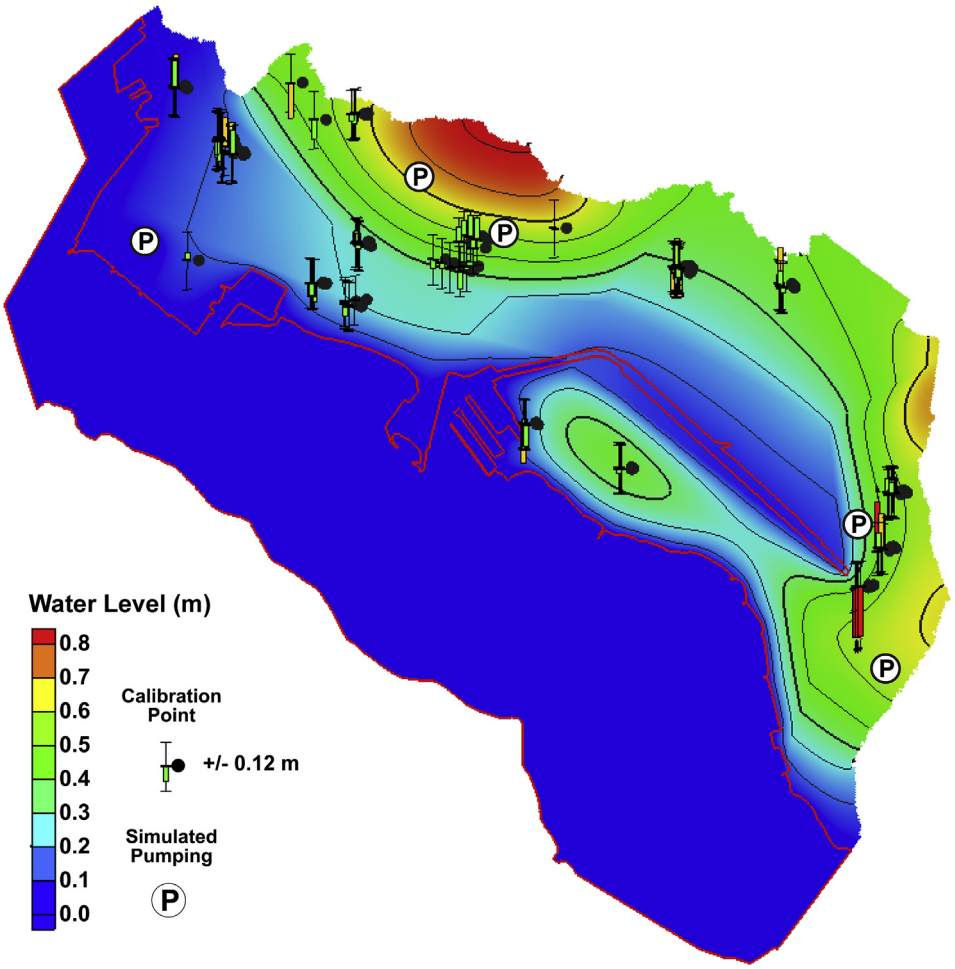

Fig. 6. Simulated water levels reported in meters relative to LMSL representing current conditions with average annual recharge and a 0-m tide stage. Circles with the letter "P" show the locations of pumping wells. Calibration points are shown to illustrate goodness of fit to observed values. Upward and downward extending bars indicate simulated water levels above and below observed levels respectively. Green bars indicate that computed values are within the model error of 12 cm and orange and red bars indicate computed values in excess of one and two standard deviations, respectively. The red line shows the extent of the coastline and the offshore boundary of study area.

SLR-induced lifting of tidally-influenced coastal water-tables. GWI represents a source of flooding separate from that of direct marine flooding, and will occur regardless of shoreline hardening. Model results indicate that SLR will have a strong influence on elevations of the coastal groundwater table. Because tidal ranges are generally normally distributed, it follows that episodic GWI will initially occur at extreme points in the tide, following which it can be expected to increase in magnitude and frequency as the elevation of built infrastructure is progressively breached at more frequently occurring tide stages.

While the main goals of this case study were focused towards assessing future vulnerabilities, results illuminated two issues of current concern for the coastal municipality. First, results reveal a potential prevalence of OSDS inundation by groundwater, and thus direct and widespread seepage of untreated sewage directly into coastal groundwater. Contamination by OSDS sites has become a growing concern as climate-change related temperature increases and unsaturated space narrowing reportedly have the potential to reduce the volume of unsaturated soil and oxygen available to treat wastewater (Cooper et al., 2016). Such reduction in sewage treatment would increase the transport of pathogens and thus jeopardize the health of the public and coastal ecosystems (Cooper et al., 2016). Additionally, this contamination will be present at the ground surface as groundwater progressively breaches the terrain. To prevent future surface exposure of contaminants, it may be necessary to remediate soil at OSDS sites that are projected to be fully submerged.

The second issue of concern is the likelihood that rainfall induced surficial flooding, commonly experienced in the study area, may result from the prevalence of narrow unsaturated space. During heavy rainfall events, narrow unsaturated space limits the amount of water that can be accommodated through infiltration. It follows that in regions where unsaturated space is narrow (less than 0.33 m), it is likely that rain induced flooding is partially the result of the full saturation of the soil. Further investigation is required to confirm this; however, if found to be true, regions projected to host narrow unsaturated space in the future can also be expected to experience increased rainfall induced flooding. This will occur in concurrence with the progressive reduction of water accommodation by storm drains due to SLR. Thus, it can be assumed that raster visualizations indicate tidally-induced chronic GWI in regions shown as flooded, and episodic rainfall induced flooding in regions shown as having narrow unsaturated space.

Based on the presented scenarios, it is envisioned that as infiltration and drainage are diminished, pools of brackish water containing urban pollutants will become increasingly widespread. Buried infrastructure (e.g., basements, cesspools, utility corridors) not designed to withstand continued submersion will experience

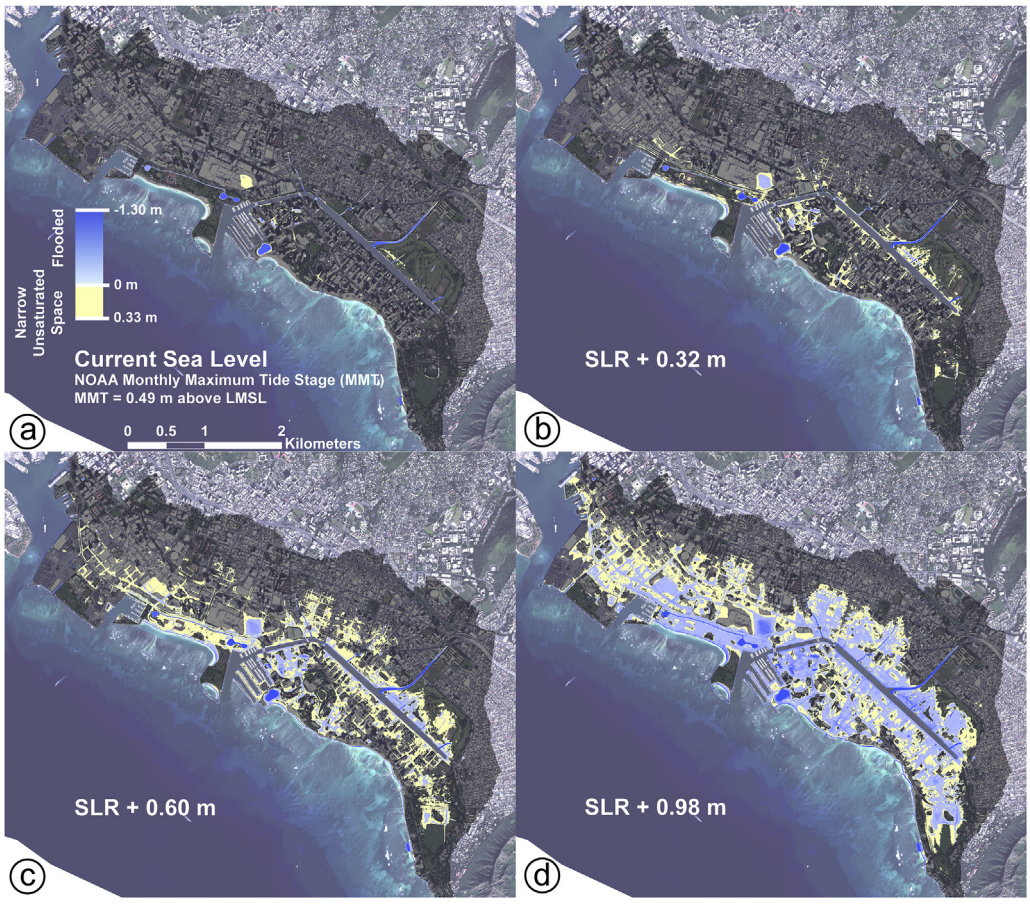

Fig. 7. Raster visualizations of simulated GWI (blue) and narrowed unsaturated space (yellow) for simulations representing a) current conditions and b) 0.32, c) 0.60, and d) 0.98 m increases in sea-level for a tide height representative of the MMT datum (0.49 m above LMSL). The study area is indicated by the shadowed region. Vertical error in the distance between terrain and groundwater is ± 20 cm.

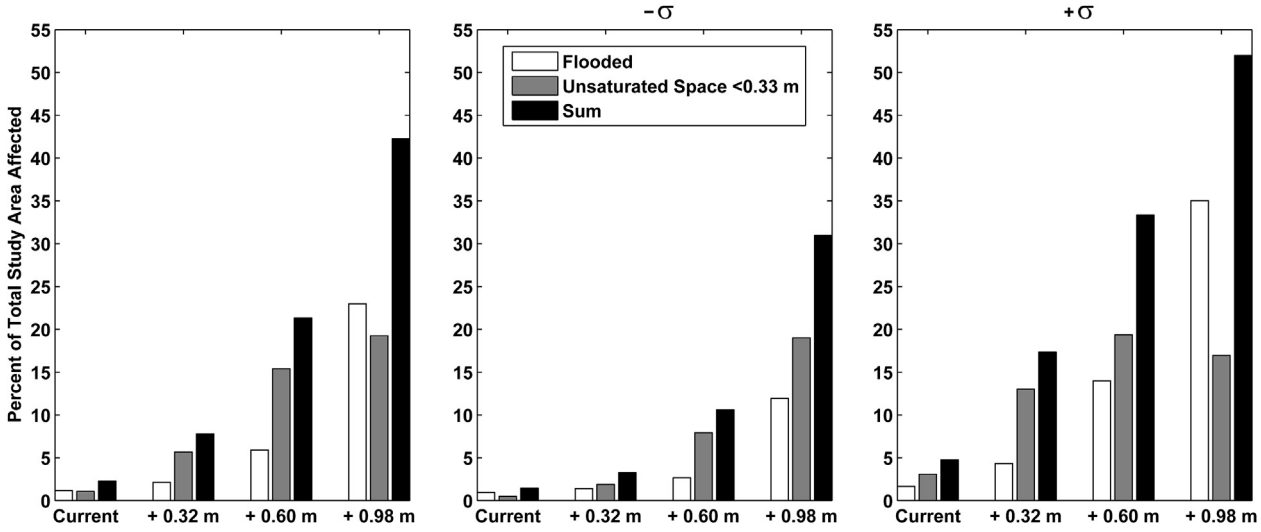

Fig. 8. Spatial calculations of study area percentages considering regions with unsaturated space narrower than 0.33 m, regions with GWI, and the sum of both. Percentages were additionally calculated for scenarios considering the error of +20 cm and −20 cm, denoted here as σ.

inundation and saltwater intrusion. These impacts present engineering challenges that endanger the economic feasibility of maintaining a dry city. Practical upgrades toward maintaining a dry city would include the installation of groundwater and stormwater pumping units, and the modification of drainage to reduce inflow of seawater during high tide. Alternatively, vulnerable areas could be redesigned to accommodate a certain amount of flooding. Adapted means of transportation, such as elevated mass-transit

Table 2
Results of the damage assessment including taxable parcel and structure real estate considering damages to the ground floor, kilometers of inundated roadway, percentage of the total number of active OSDS sites not compliant with current construction regulations, and the number of OSDS sites fully submerged to the ground surface.

Sea level rise projection	Taxable real estate (property and structures)	Inundated roadway (km)	Percentage of total 259 OSDS sites likely inundated	Number of cesspools fully submerged
Current	$185,319,692	0.02	86%	1
+0.32 m	$380,638,276	1.20	90%	1
+0.60 m	$1,149,800,027	10.99	91%	5
+0.98 m	$4,968,484,196	47.55	91%	39

systems, may be necessary, considering the prevalence of GWI along heavily utilized roadways shown in accompanying simulations. In any case, it will be necessary that submerged infrastructure be constructed to withstand constant submersion in saline waters, and that OSDS reliant properties lacking sufficiently thick unsaturated space be connected to municipal sewage treatment systems.

5. Conclusion

Over the 21st century, sea level is expected to rise to magnitudes that will result in extensive damage to dense networks of buried and surface infrastructure that exist across heavily developed coastlines. The inundation of low-lying areas and buried infrastructure by tidally influenced groundwater has already become chronically damaging in urban municipalities along the East Coast of the United States. In preparation for more extreme and frequent flood events, the identification of vulnerabilities is a necessary step toward designing workable solutions.

This case study illustrates the need to consider coastal groundwater fluxions in the simulation of SLR induced flooding and presents a regionally flexible methodology in which to do so. The methodology is specifically geared for use in heavily-developed coastal regions owing to the generally increased well availability and public accessibility of required data sets. The production of flood simulations combines groundwater monitoring, quasi-3 dimensional hydrologic modeling (MODFLOW-2005), 1-D analytical evaluation of tidal influence, and terrain modeling. The model output consists of raster data sets that specify the elevation of the water-table either above or below the simulated terrain, which can be seamlessly integrated into geospatial platforms to conduct various hazard analyses.

For proof of concept, this study applies the methodology to the Waikiki area of Honolulu, Hawaii. Here we construct flood simulations that consider current conditions and future elevations of sea-level at 0.32, 0.60, and 0.98 m, and a tide stage representative of the mean maximum monthly tide elevation (0.49 m above LMSL). Tidal influence was estimated across the study area based on continuous water-level monitoring in three wells.

The hydrologic model simulation of current water-table elevations was calibrated using data from monitoring wells in addition to 95 discrete water-level measurements compiled from Department of Health Leaky Underground Storage Tank reports. The calibrated model produced a root-mean-squared residual of 12 cm between observed and simulated groundwater levels. Following calibration, the influence of SLR on water-tables was simulated by specifying the modeled ocean elevations for future scenarios of SLR.

Results indicate that approximately 1.1% of the 13 km^2 study area presently has narrow unsaturated space of less than 0.33 m. SLR of 0.98 m raises this extent to 19.3% and produces GWI over 23.0% of the study area. It follows that under 0.98 m of SLR, nearly half (~42%) of the region will likely experience either chronic GWI during elevated stages of the tide, or episodic flooding induced by heavy rainfall. The corresponding hazard assessment indicates that the currently narrow state of unsaturated space likely causes inundation of 86% of 259 active OSDS sites located across the study area, and threatens to fully submerge 39 OSDS sites by the end of the century. This suggests that sewage based contamination is currently ongoing across the study area. If contamination is indeed ongoing and remains unchecked, serious public health ramifications could ensue as waters progressively breach the surface and come into contact with local residents and the millions of visitors who travel to Waikiki each year.

Acknowledgments

This work is sponsored by the University of Hawaii Sea Grant Program [Award Number NA140AR4170071] and by the Honolulu Board of Water Supply [Award Number C16545003]. We gratefully acknowledge the Hawaii State Department of Health, the U.S. Geological Survey, the Department of Land and Natural Resources, Pacific Islands Climate Science Center, the Honolulu Board of Water Supply, and the University of Hawaii Coastal Geology Group. This is SOEST contribution number 9946.

References

Balaraman, K., 2016. Sewage Floods Likely to Rise [WWW Document]. Clim. Wire. http://www.scientificamerican.com/article/sewage-floods-likely-to-rise/# (accessed 20 October 2016).
Bierbaum, R., Smith, J.B., Lee, A., Blair, M., Carter, L., Chapin III, F.S., Fleming, P., Ruffo, S., Stults, M., McNeeley, S., 2013. A comprehensive review of climate adaptation in the United States: more than before, but less than needed. Mitig. Adapt. Strateg. Glob. Chang. 18, 361–406.
Carlson, E., May 5, 2016. Pacific Region Geodetic Advisor for NOAA's National Geodetic Survey. Email Communication.
Church, J.A., Clark, P.U., Cazenave, A., Gregory, J.M., Jevrejeva, S., Levermann, A., Merrifield, M.A., Milne, G.A., Nerem, R.S., Nunn, P.D., 2013. Sea level change. In: Climate Change 2013: the Physical Science Basis. Contribution of Working Group I to the Fifth Assessment Report of the Intergovernmental Panel on Climate Change (RPRT). PM Cambridge University Press.
City and County of Honolulu (CCH), 2016. CCH Data Download Site: Structures_Facilities [WWW Document]. http://gis.hicentral.com/datadictionary/Structure_Nga.htm (accessed 20 October 2016).
Cooper, J.A., Loomis, G.W., Amador, J.A., 2016. Hell and high water: diminished septic system performance in coastal regions due to climate change. PLoS One 11, e0162104.
DeConto, R.M., Pollard, D., 2016. Contribution of Antarctica to past and future sea-level rise. Nature 531, 591–597.
Department of Business: Economic Development and Tourism, 2003. The Economic Contribution of Waikiki [WWW Document]. http://files.hawaii.gov/dbedt/economic/data_reports/e-reports/econ_waikiki.pdf (accessed 20 October 2016).
Department of Health, 2004. Hawaii Administrative Rules, Title 11. Department of Health, Chapter 62, Wastewater Systems.
Doherty, J., 2008. Groundwater Data Utilities. Watermark Numer. Comput, Brisbane. Aust.
Engott, J.A., Johnson, A.G., Bassiouni, M., Izuka, S.K., 2015. Spatially Distributed Groundwater Recharge for 2010 Land Cover Estimated Using a Water-budget Model for the Island of O'ahu, Hawai'i. Scientific Investigations Report 2015-5010 (RPRT). US Geological Survey.
Ferrall, C.C., 1976. Subsurface Geology of Waikiki, Moiliili and Kakaako with Engineering Application. University of Hawaii, Manoa.
Finstick, S.A., 1996. Subsurface Geology and Hydrogeology of Downtown Honolulu with Engineering and Environmental Implications. Water Resources Research Center, University of Hawaii at Manoa.
Firing, Y.L., Merrifield, M.A., 2004. Extreme sea level events at Hawaii: influence of mesoscale eddies. Geophys. Res. Lett. 31.
Gillis, J., 2016. Flooding of Coast, Caused by Global Warming, Has Already Begun. New York Times.

Gingerich, S.B., Oki, D.S., 2000. Ground Water in Hawaii Fact Sheet 126-00. US Geological Survey.
Gonneea, M.E., Mulligan, A.E., Charette, M.A., 2013. Climate-driven sea level anomalies modulate coastal groundwater dynamics and discharge. Geophys. Res. Lett. 40, 2701–2706.
Gornitz, V., Couch, S., Hartig, E.K., 2001. Impacts of sea level rise in the New York City metropolitan area. Glob. Planet. Change 32, 61–88. http://dx.doi.org/10.1016/S0921-8181(01)00150-3.
Gregory, K., 2013. Where Streets Flood with the Tide, a Debate over City Aid. New York Times.
Harbaugh, A.W., 2005. MODFLOW-2005, the US Geological Survey Modular Ground-water Model: the Ground-water Flow Process. US Geological Survey Reston, VA, USA.
Honolulu Board of Water Supply (HBWS), 2005. John a. Burns School of Medicine Kaka'ako, O'ahu, Hawai'I Kaka'ako Cold Seawater Cooling System Injection Well UIC Application UO-2287.
Horton, R.E., 1933. The role of infiltration in the hydrologic cycle. Eos Trans. Am. Geophys. Union 14, 446–460.
Izuka, S.K., Engott, J.A., Bassiouni, M., Johnson, A.G., Miller, L.D., Rotzoll, K., Mair, A., 2016. Volcanic Aquifers of Hawai'i—hydrogeology, Water Budgets, and Conceptual Models. U.S. Geological Survey Scientific Investigations. Report 2015–5164.
Langevin, C.D., Shoemaker, W.B., Guo, W., 2003. SEAWAT-2000: a Version of MODFLOW-2000 with the Variable-density Flow Process and the Integrated MT3DMS Transport Process. US Geological Survey Open-File (Report).
Li, L., Barry, D.A., 2000. Wave-induced beach groundwater flow. Adv. Water Resour. 23, 325–337.
Macdonald, G.A., Abbott, A.T., Peterson, F.L., 1983. Volcanoes in the Sea: the Geology of Hawaii. University of Hawaii Press.
National Oceanic and Atmospheric Administration (NOAA) Digital Coast (NOAA b), 2016. Digital Coast [WWW Document]. https://coast.noaa.gov/digitalcoast/ (accessed 20 October 2016).
National Oceanic and Atmospheric Administration (NOAA) Tides & Currents (NOAA a), 2016. Tide Station 1612340 Station Info [WWW Document]. http://tidesandcurrents.noaa.gov/inventory.html?id=1612340 (accessed 20 October 2016).
National Oceanic and Atmospheric Administration (NOAA c), 2016. Station Data Inventory: BERETANIA PUMP STATION 7, HI US, GHCND: USC00510211 [WWW Document]. http://www.ncdc.noaa.gov/cdo-web/datasets/NORMAL_MLY/stations/GHCND:USC00510211/detail (accessed 20 October 2016).
National Research Council (NRC), 2011. National Security Implications of Climate Change for U.S. Naval Forces. National Academies Press, Washington. D.C.
Nerem, R.S., Chambers, D., Choe, C., Mitchum, G.T., 2010. Estimating mean sea level change from the TOPEX and jason altimeter missions. Mar. Geod. 33 http://dx.doi.org/10.1080/01490419.2010.491031.
New Jersey Department of Environmental Protection (NJDEP), 2013. Christie Administration Announces Post–superstorm Sandy Flood Mitigation Studies by New Jersey Universities [WWW Document]. http://www.state.nj.us/dep/newsrel/2013/13_0091.htm.
Nicholls, R.J., 1995. Coastal megacities and climate change. GeoJournal 37, 369–379.
Oki, D.S., 2005. Numerical Simulation of the Effects of Low-permeability Valley-fill Barriers and the Redistribution of Ground-water Withdrawals in the Pearl Harbor Area, Oahu, Hawaii. Scientific Investigations Report 2005-5253. US Geological Survey.
Oki, D.S., Souza, W.R., Bolke, E.L., Bauer, G.R., 1998. Numerical analysis of the hydrogeologic controls in a layered coastal aquifer system, Oahu, Hawaii, USA. Hydrogeol. J. 6, 243–263.
Photo Science Inc, 2013. Airborne Topographic LiDAR Report: O'ahu, Hawai'i. Post Flight Aerial Acquisition and Calibrated Report to USGS. Contract No. G10PC00026.
Ponte, R.M., 1994. Understanding the relation between wind-and pressure-driven sea level variability. J. Geophys. Res. Ocean. 99, 8033–8039.
Prothero, A., 2013. What South Florida's Spring Tide (Or King Tide) Looks like. WLRN-TV. WWW Document. http://wlrn.org/post/what-south-floridas-spring-tide-or-king-tide-looks (accessed 20 October 2016).
Rotzoll, K., El-Kadi, A.I., 2007. Numerical Ground-water Flow Simulation for Red Hill Fuel Storage Facilities, NAVFAC Pacific, Oahu, Hawaii (JOUR). University of Hawaii & Water Resources Research Center, prepared for TEC Inc., Honolulu, Hawaii.
Rotzoll, K., Fletcher, C.H., 2013. Assessment of groundwater inundation as a consequence of sea-level rise. Nat. Clim. Chang. 3, 477–481.
Savonis, M.J., Burkett, V.R., Potter, J.R., 2008. Impacts of Climate Change and Variability on Transportation Systems and Infrastructure: Gulf Coast Study, Phase I (JOUR). US Climate Change Science Program.
Sherman, C.E., Fletcher, C.H., Rubin, K.H., 1999. Marine and meteoric diagenesis of Pleistocene carbonates from a nearshore submarine terrace, Oahu, Hawaii. J. Sediment. Res. 69.
Sherman, C.E., Fletcher, C.H., Rubin, K.H., Simmons, K.R., Adey, W.H., 2014. Sea-level and reef accretion history of Marine Oxygen Isotope Stage 7 and late Stage 5 based on age and facies of submerged late Pleistocene reefs, Oahu. Hawaii. Quat. Res. 81, 138–150. http://dx.doi.org/10.1016/j.yqres.2013.11.001.
Souza, W.R., Voss, C.I., 1987. Analysis of an anisotropic coastal aquifer system using variable-density flow and solute transport simulation. J. Hydrol. 92, 17–41.
Spada, G., Bamber, J.L., Hurkmans, R., 2013. The gravitationally consistent sea- level fingerprint of future terrestrial ice loss. Geophys. Res. Lett. 40, 482–486.
Spanger-Siegfried, E., Fitzpatrick, M., Dahl, K., 2014. Encroaching Tides: How Sea Level Rise and Tidal Flooding Threaten US East and Gulf Coast Communities over the Next 30 Years. Cambridge, MA.
State of Hawaii Office of Planning (SHOP), 2016. Hawaii Statewide GIS Program: Download GIS Data [WWW Document]. http://planning.hawaii.gov/gis/download-gis-data/ (accessed 20 October 2016).
Stearns, H.T., 1935. Pleistocene shore lines on the islands of Oahu and Maui. Hawaii. Geol. Soc. Am. Bull. 46, 1927–1956.
Stearns, H.T., Vaksvik, K.N., 1935. Geology and Ground-water Resources of the Island of Oahu, Hawaii. Maui Publishing Company, Limited.
Sterling, R., Nelson, P., 2013. City Resiliency and Underground Space Use. Adv. Undergr. Sp. Dev. Singapore ACUUS.
Strauss, B.H., Ziemlinski, R., Weiss, J.L., Overpeck, J.T., 2012. Tidally adjusted estimates of topographic vulnerability to sea level rise and flooding for the contiguous United States. Environ. Res. Lett. 7, 14033.
Sweet, W.V., Park, J., 2014. From the extreme to the mean: acceleration and tipping points of coastal inundation from sea level rise. Earth's Futur 2, 579–600.
Sweet, W.V., Kopp, R.E., Weaver, C.P., Obeysekera, J., Horton, R.M., Thieler, E.R., Zervas, C., 2017. Global and Regional Sea Level Rise Scenarios for the United States. NOAA Technical Report NOS CO -OPS 083. Maryland, Silver Spring.
Sweet, W.V., 2014. Sea Level Rise and Nuisance Flood Frequency Changes Around the United States. NOAA Technical Report NOS CO-OPS 073.
US Army Corps of Engineers (USACE), 2013. Coastal Risk Reduction and Resilience: Using the Full Array of Measures.
Veiga, C., 2014. Miami Beach to Spend up to $400 Million to Deal with Flooding Issues. Miami Her.
Whittier, R.B., El-Kadi, A., 2014. Human Health and Environmental Risk Ranking of On-site Sewage Disposal Systems for the Hawaiian Islands of Kauai, Molokai, Maui, and Hawaii. Final report prepared for State of Hawai'i Department of Health, Safe Drinking Water Branch.
Whittier, R.B., El-Kadi, A.I., 2009. Human and Environmental Risk Ranking of Onsite Sewage Disposal Systems, Final. Department of Geology & Geophysics, University of Hawaii at Manoa.
Whittier, R.B., Rotzoll, K., Dhal, S., El-Kadi, A.I., Ray, C., Chang, D., 2010. Groundwater source assessment program for the State of Hawaii, USA: methodology and example application. Hydrogeol. J. 18, 711–723.
Wu, J., Zhang, R., Yang, J., 1996. Analysis of rainfall-recharge relationships. J. Hydrol. 177, 143–160.
Yin, B., Hou, Y., Cheng, M., Su, J., Lin, M., Li, M., El-Sabh, M.I., 2001. Numerical study of the influence of waves and tide-surge interaction on tide-surges in the Bohai Sea. Chin. J. Oceanol. Limnol. 19, 97–102.